A dilute Cu(Ni) alloy for synthesis of large-area Bernal stacked bilayer graphene using atmospheric pressure chemical vapour deposition

M. J. Madito,[1] A. Bello,[1] J. K. Dangbegnon,[1] C. J. Oliphant,[2] W. A. Jordaan,[2] D. Y. Momodu,[1] T. M. Masikhwa,[1] F. Barzegar,[1] M. Fabiane,[1,3] and N. Manyala[1,a)]

[1]*Department of Physics, Institute of Applied Materials, SARCHI Chair in Carbon Technology and Materials, University of Pretoria, Pretoria 0028, South Africa*
[2]*National Metrology Institute of South Africa, Private Bag X34, Lynwood Ridge, Pretoria 0040, South Africa*
[3]*Department of Physics, National University of Lesotho, P.O. Roma 180, Lesotho*

A bilayer graphene film obtained on copper (Cu) foil is known to have a significant fraction of non-Bernal (AB) stacking and on copper/nickel (Cu/Ni) thin films is known to grow over a large-area with AB stacking. In this study, annealed Cu foils for graphene growth were doped with small concentrations of Ni to obtain dilute Cu(Ni) alloys in which the hydrocarbon decomposition rate of Cu will be enhanced by Ni during synthesis of large-area AB-stacked bilayer graphene using atmospheric pressure chemical vapour deposition. The Ni doped concentration and the Ni homogeneous distribution in Cu foil were confirmed with inductively coupled plasma optical emission spectrometry and proton-induced X-ray emission. An electron backscatter diffraction map showed that Cu foils have a single (001) surface orientation which leads to a uniform growth rate on Cu surface in early stages of graphene growth and also leads to a uniform Ni surface concentration distribution through segregation kinetics. The increase in Ni surface concentration in foils was investigated with time-of-flight secondary ion mass spectrometry. The quality of graphene, the number of graphene layers, and the layers stacking order in synthesized bilayer graphene films were confirmed by Raman and electron diffraction measurements. A four point probe station was used to measure the sheet resistance of graphene films. As compared to Cu foil, the prepared dilute Cu(Ni) alloy demonstrated the good capability of growing large-area AB-stacked bilayer graphene film by increasing Ni content in Cu surface layer. © 2016 AIP Publishing LLC.
[http://dx.doi.org/10.1063/1.4939648]

I. INTRODUCTION

Graphene as a two-dimensional structured carbon material has attracted many researchers due to its fascinating properties and potential applications.[1–4] However, its zero band gap restricts some of its applications.[1] One of the approaches of opening the band gap in graphene is synthesizing a Bernal (AB) stacked bilayer graphene that is known to exhibit a tunable band gap of up to 0.25 eV.[2–4] Amongst the common approaches used to produce AB-stacked bilayer graphene films are the chemical vapour deposition (CVD) which has attracted tremendous research activities due to its ability to produce wafer-scale high-quality graphene films with a controllable number of layers.[5–7] In CVD graphene growth, metal substrates are used to promote graphene synthesis by a surface growth mechanism or by segregation (precipitation).[8,9] Metal substrates commonly used for CVD graphene growth include nickel (Ni) and copper (Cu).[8,9]

Nevertheless, for a CVD bilayer graphene, these metal substrates have limitations or challenges. For instance, a bilayer graphene film obtained on Ni has large traces of multi-layers, and on Cu only fraction of the bilayer graphene film has AB stacking order.[4,9,10] Interestingly, a binary Cu-Ni metal alloy has shown a capacity of growing a large-area

AB-stacked bilayer graphene film in comparison to pure Cu.[5,6] This was demonstrated by Chen *et al.*,[6] using commercial Cu-Ni alloy foils with 31.0 wt. % Ni, 67.8 wt. % Cu composition, and Liu *et al.*,[5] using Cu(1200 nm)/Ni(400 nm) thin films deposited onto SiO$_2$ substrate. The good capability of Cu-Ni alloy of growing a large-area AB-stacked bilayer graphene film as compared to Cu demonstrated a lower hydrocarbon decomposition rate (i.e., weak supply of active carbon species which materialise into graphene) of Cu surface at an optimized hydrocarbon pressure in CVD graphene growth process.[5] It is believed that active impurity atoms in Cu segregate to the Cu surface during annealing and enhance the hydrocarbon decomposition rate of Cu,[4] but the level of enhancement is related to the surface concentration of the segregated impurity atoms and the atom-atom interaction energy. In addition, as compared to Cu, Ni has higher carbon solubility and decomposition rate of methane (i.e., strong supply of active carbon species which materialise into graphene), hence it enhances the hydrocarbon (methane) decomposition rate in Cu-Ni alloy during CVD graphene growth.[5] To tune the hydrocarbon decomposition rate of Cu by doping Cu with Ni, the maximum surface concentration of Ni that will be segregated during CVD graphene growth is important and is determined by the concentration of Ni in Cu (i.e., Ni bulk concentration) and the segregation driving energy (segregation energy).[11] Liu *et al.*[5] have shown that

a)Author to whom correspondence should be addressed. Electronic mail: ncholu.manyala@up.ac.za

Cu(1200 nm)/Ni(400 nm) films having a surface layer composition of >97 at. % Cu and <3 at. % Ni grow a wafer-scale AB-stacked bilayer graphene in CVD. Now, for a Cu foil to have a surface layer composition of about 97 at. % Cu and 3 at. % Ni through Ni segregation during graphene growth in the temperature range of 900–1000 °C, it should have about 0.5 at. % Ni bulk concentration and Ni segregation driving energy of about 30 kJ/mol. Consequently, we propose the use of homogeneous dilute Cu(0.5 at. % Ni) foil for large-area AB-stacked bilayer graphene growth in CVD. Dilute Cu(Ni) foils for CVD multilayer graphene growth have not received much attention. Nonetheless, studies have used pure Cu foils,[8] Cu/Ni thin films,[5,9,13] and non-dilute commercial Cu-Ni foils (i.e., Cu(88.0 wt. %)-Ni(9.9 wt. %)[14] and Cu(67.8 wt. %)-Ni(31.0 wt. %)[6]) in CVD for graphene growth. A bilayer graphene film obtained on pure Cu foil is known to have islands of bilayer with monolayer background and significant fraction of non-AB stacking,[10] on Cu(1200 nm)/Ni(400 nm) thin films is known to grow over a large-area with AB stacking, and for non-dilute Cu-Ni foils a CVD graphene growth is known to dominate from segregation/precipitation process, which could lead to a variation in the uniformity of the bilayer graphene over large areas and a significant fraction of non-AB stacking in bilayer graphene.[14]

Despite the previous works on growth of AB-stacked bilayer graphene films using CVD system,[6,9–15] a controllable CVD growth of a continuous large-area high-quality AB-stacked bilayer graphene remains a challenge for different laboratories with CVD set-up for graphene growth. This work is aimed at preparation and analysis of dilute Cu(Ni) foils for growth of large-area AB-stacked bilayer graphene using atmospheric pressure chemical vapour deposition (AP-CVD).

II. EXPERIMENTAL

A. Thermal deposition and annealing

Few Cu foil samples ($\sim$30 × 30 mm^2) (to be prepaid the same way) were obtained from a high purity (99.8%) 25 μm thick annealed Cu foil from Alfa Aesar. Samples were immersed in aqueous nitric acid for 30 s to dissolve surface impurities on foils, then in distilled water followed by an ultra-sonic bath with acetone and isopropanol and dry-blowing with N$_2$ to remove water residues.[16] The cleaned Cu foils were loaded in a vacuum chamber of a thermal evaporator for Ni deposition. A thin layer of high purity (99.99%) Ni (116 nm) was thermally evaporated onto Cu foil sample at a rate of 1 Å/s in a vacuum chamber with a pressure of 3×10^{-3} Pa. The deposition of a thin layer of Ni was repeated on extra three Cu foil samples. After evaporation, Cu/Ni samples were loaded in AP-CVD quartz tube under argon atmosphere. Samples were annealed at 950 °C for 8 h with argon flow rate of 500 sccm to obtain a homogeneous distribution of Ni concentration in Cu foils. For the 950 °C and 8 h annealing conditions, the concentration distribution (C) of Ni in Cu foil with a thickness l and the surface located at $x = 0$, where the Ni source layer with a thickness h is restricted, was calculated in terms of diffusion depth x using Fick's solution for finite systems (see Fig. 1(a))[17]

$$C = \frac{1}{2} C_0 \sum_{n=-\infty}^{\infty} \mathrm{erf}\left(\frac{h + 2nl - x}{2\sqrt{Dt}}\right) + \mathrm{erf}\left(\frac{h - 2nl + x}{2\sqrt{Dt}}\right), \quad (1)$$

where C_0 is the initial concentration of Ni on the Cu surface, $D = D_0 \exp(-Q/RT)$ is the diffusion coefficient (D_0 is the pre-exponential factor, Q is the activation energy ($D_0 = 7.0 \times 10^{-5}$ m^2/s and $Q = 225.0$ kJ/mol for Ni diffusion in Cu[18]), R is the gas constant, and T is the temperature).

The annealing process yielded Ni concentration distribution in 25 μm thick Cu foil that is 99.8% uniform (see Fig. 1(a) calculation for a Cu foil sample 1 in Table I). After annealing at 950 °C, a 10.0 kV primary electron beam in scanning electron microscopy (SEM) was scanned across the Cu foil surface to obtain its micro-structural image as shown in Fig. 1(b) and shows the average grain size of 35.7 μm. Before and after deposition of the Ni films onto the Cu foils, the masses of the samples were measured with Denver instrument balance (model SI-234) with repeatability or standard deviation of <±0.1 mg. After annealing, the masses of the samples were measured again and found to have increased, and from Ni masses the concentrations were found as listed in Table I. An ICP-OES (inductively coupled plasma optical emission spectrometry) spectrometer was used to confirm the Ni concentrations listed in Table I. For
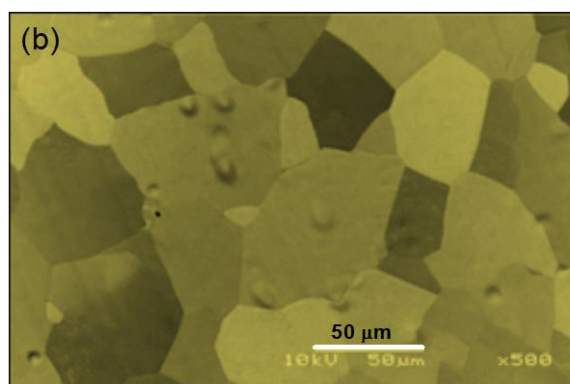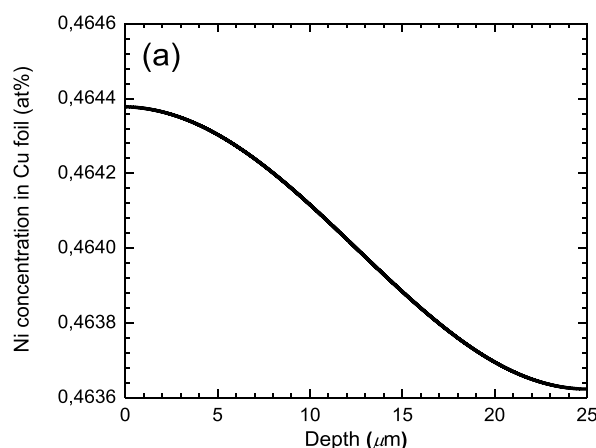

FIG. 1. (a) Ni concentration distribution as a function of diffusion depth in 25 μm thick Cu foil. (b) The micro-structure image of annealed Cu foil surface.

TABLE I. The masses of the samples and Ni added in Cu foils and the corresponding Ni concentrations.

Cu foils samples	Cu foils masses pre-deposition (± 0.1 mg)	Cu foils masses after deposition (± 0.1 mg)	Cu foils masses after annealing (± 0.1 mg)	Ni masses in Cu foils after annealing (± 0.1 mg)	Ni doped concentration (at. %)
1	285.4	286.9	286.6	1.2	0.455
2	268.1	269.3	269.6	1.5	0.606
3	262.0	263.3	263.4	1.4	0.579
4	251.0	252.2	252.5	1.5	0.647

instance, a piece of a Cu foil with a mass of 47.1 mg was cut from a Cu foil sample 1 and analysed with an ICP-OES spectrometry and was found to have a Ni amount with a mass of 0.199 mg (equivalent to 0.457 at. %).

Ni doped (i.e., Cu(0.46 at. % Ni, sample 1 in Table I)) and un-doped Cu foils were loaded in AP-CVD at a centre of a quartz tube for bilayer graphene growth (see a schematic view of AP-CVD setup in Fig. 2(a)). Figure 2(b) shows a temperature profile of AP-CVD measured directly inside quartz tube centre located at the furnace centre with external chromel–alumel thermocouple (type K), and the measured temperature was calibrated in terms of true sample temperature for graphene growth.

B. Bilayer graphene synthesis and transfer onto SiO$_2$

Pre-growth of graphene, Cu and Cu(0.46 at. % Ni) foils were annealed under Ar (300 sccm) and H$_2$ (100 sccm) flow for 60 min (see Fig. 2(b)) to obtain a clean and uniform surface. After annealing, the graphene was synthesised at 920 °C from a mixture of gases, Ar (300sccm): H$_2$ (9 sccm): CH$_4$ (10 sccm)[19] for exactly 15 min. Immediately after growth, the CH$_4$ flow was stopped and samples were rapidly cooled down by pushing the quartz tube to the cooler region of the furnace. At less than 80 °C, samples were off loaded from AP-CVD quartz tube and transferred onto 300 nm thick SiO$_2$/Si substrates.

In the transfer, a thin layer of poly methyl methacrylate (PMMA) (average Mw ∼996 000 by gel permeation chromatography (GPC)) dissolved in chlorobenzene with a concentration of 46 mg/ml was spin-coated on the as-grown graphene on both Cu and Cu(Ni) foils at 3000 rpm for 30 s. PMMA/graphene/(Cu and Cu(Ni)) foil samples were placed in 1 M iron nitrate to etch off Cu and Cu(Ni).[5,6] PMMA/

graphene films floated in the etchant after the foils were etched. These films were then transferred using a polyethylene terephthalate (PET) to the 5% hydrochloride (HCl), then, deionized (DI) water to dissolve the iron nitrate,[5] and subsequently the PMMA/graphene films were transferred onto SiO$_2$ substrates. Finally, PMMA was removed by placing samples in an acetone bath for 6 h.[20]

C. Characterizations

Proton-induced X-ray emission (PIXE) was used to map Ni distribution in Cu and Cu-Ni foils. An additional high purity (99.999%) Cu grid was used for mapping Cu signal. A beam energy of 3.0 MeV and target current of 200 pA were used for analysis. Electron backscatter diffraction (EBSD) analysis of a Cu foil was performed in a LEO 1525 field-emission gun scanning electron microscope at an acceleration voltage of 25 kV using the Oxford INCA crystal software. The X-ray diffraction (XRD) pattern of Cu foil was collected using an XPERT-PRO diffractometer (PANalytical BV, Netherlands) with reflection geometry at 2θ values ranging from 30° to 70° with a step size of 0.01°. Co $K1\alpha$ radiation with a wavelength of 1.7890 Å was used as the X-ray source, and a tube was operated at 50 kV and 30 mA. Time-of-flight secondary ion mass spectroscopy (TOF-SIMS) depth profiling was performed on Cu and Cu-Ni foils using the TOF-SIMS5 Ion-TOF system. The mass spectra were calibrated to the following mass peaks in positive mode: Al, Na, Ni, Fe, Si, C, C$_2$H$_5$, K, and Cu. For analysis, a Ga$^+$ primary ion beam was used, and for sputtering a Cs$^+$ ion beam was used. The analyses were carried out over an area of 500×500 μm^2 and sputter gun area of 1000×1000 μm^2 and time interval of 6 s. The graphene
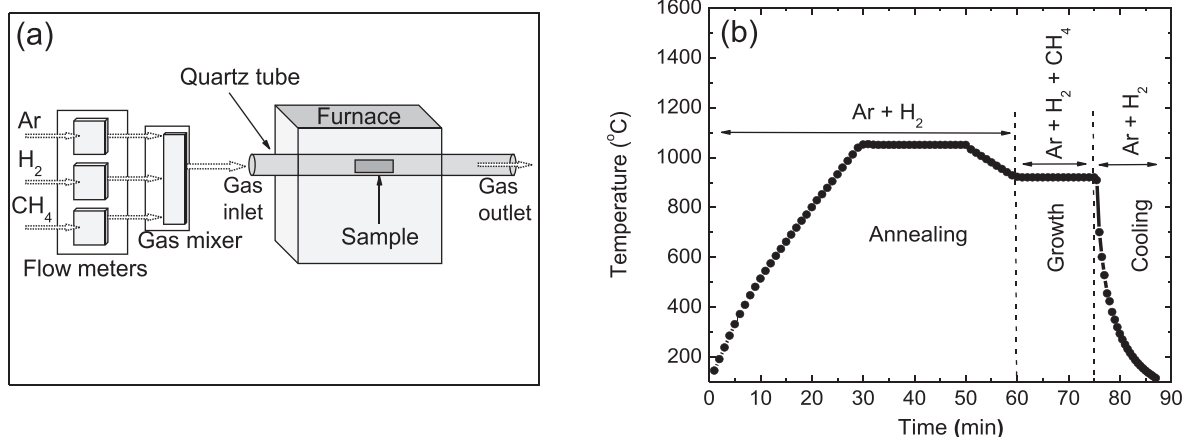

FIG. 2. (a) A schematic view of AP-CVD setup. (b) A temperature profile of AP-CVD measured directly inside quartz tube centre.
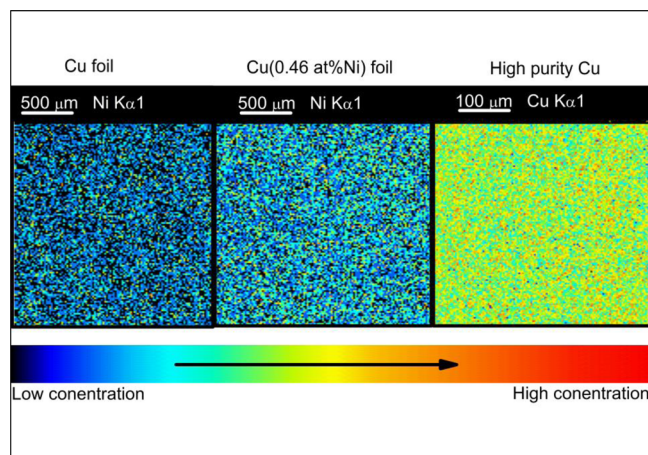
FIG. 3. PIXE maps of Ni distribution in Cu, Cu(0.46 at. % Ni) foil and high purity Cu grid.

films transferred onto SiO_2 substrates were characterized with WITec Alpha 300 micro-Raman imaging system with 532 nm excitation laser. Raman spectra were measured at room temperature with the laser power set below 2 mW in order to minimize heating effects. The graphene film sheet resistance measurements were carried out in ambient conditions (i.e., in air at room temperature and pressure) using a Signatone four point probe station. A DC current in the range of 0–1.7 mA was used. The electron diffraction pattern of prepared graphene film was obtained with high-resolution transmission electron microscopy (HRTEM) (Jeol JEM-2100F Field Emission Electron Microscope, with a maximum analytical resolution of 200 kV and a probe size under 0.5 nm).

III. RESULTS

A. PIXE, EBSD, and XRD analysis of Cu and Cu(Ni) foils

Figure 3 shows PIXE maps for Ni distribution in Cu, Cu(0.46 at. % Ni) foil and high purity Cu grid. A PIXE map for Cu(0.46 at. % Ni) foil shows high Ni concentration as compared to that of Cu foil, as expected. PIXE maps suggest

that Ni distribution is uniform through foils. Figure 4(a) shows an EBSD map of Cu foil which shows a continuous crystallographic surface composed of (001) orientation in accordance with the inverse pole figure orientation component colouring scheme (the bottom inset to Fig. 4(a)), and the top inset to Fig. 4(a) shows the SEM image of a Cu foil surface that is mapped out with an EBSD. In Fig. 4(a), the scale bar is 30 μm which is about the same order of magnitude as the average grains size of the foil (i.e., 35.7 μm); hence, few grains of a Cu foil are expected to be captured within the EBSD image. Therefore, an EBSD map shows that annealed Alfa Aesar Cu foil used for graphene growth has a preferential (001) surface orientation. The EBSD data are supported by XRD data (Fig. 4(b)) showing a single diffraction intensity peak of Cu(002) orientation which is parallel to Cu(001) orientation. Nonetheless, an XRD data are not restricted to surface information, but rather bulk information hence the data are not used to obtain surface grains crystallographic information.

B. TOF-SIMS analysis of Cu and Cu(Ni) foils

Figure 5 shows depth profiles of Cu and Cu(0.46 at. % Ni) foils after annealing under conditions similar to that of graphene growth, where some of the impurities (Al, Na, Ni, Fe, Si, C_2H_5, and K) in Cu can be seen in surface and bulk regions of the samples. *In Cu foil*: Fig. 5(a) depth profile shows the presence of impurities in the bulk, and some of these impurities have higher intensities in the surface region of a foil. Though the impurities show high intensities in TOF-SIMS, they do not necessarily show high surface concentrations, since they have strong signals in TOF-SIMS. Interestingly, Ni impurity with almost zero intensity ratios in the bulk shows higher intensity ratio in the surface region and that demonstrates Ni surface precipitation/segregation capability. Similarly, *in Cu(0.46 at. % Ni) foil*: Fig. 5(b) depth profile shows the presence of impurities in both bulk and surface regions of a foil. In contrast to Cu foil, Ni has higher intensity ratio in the bulk and surface region of a foil and that demonstrates an increase in Ni bulk concentration
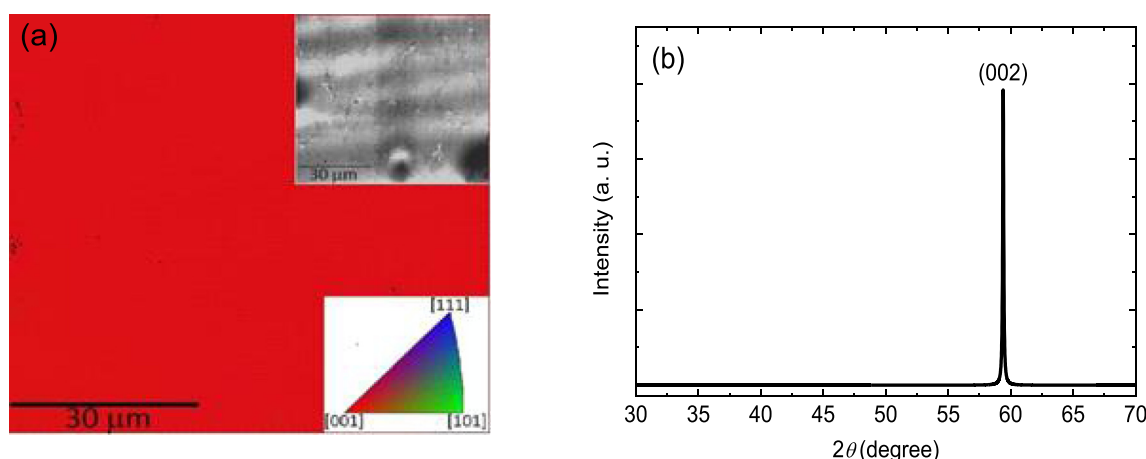

FIG. 4. (a) An EBSD map of high temperature annealed Alfa Aesar Cu foils for graphene growth (the top-right inset is SEM image of an area mapped out with EBSD, and the bottom-right inset is the EBSD map corresponding inverse pole figure orientation component colouring scheme). (b) XRD data of the annealed Cu foil.
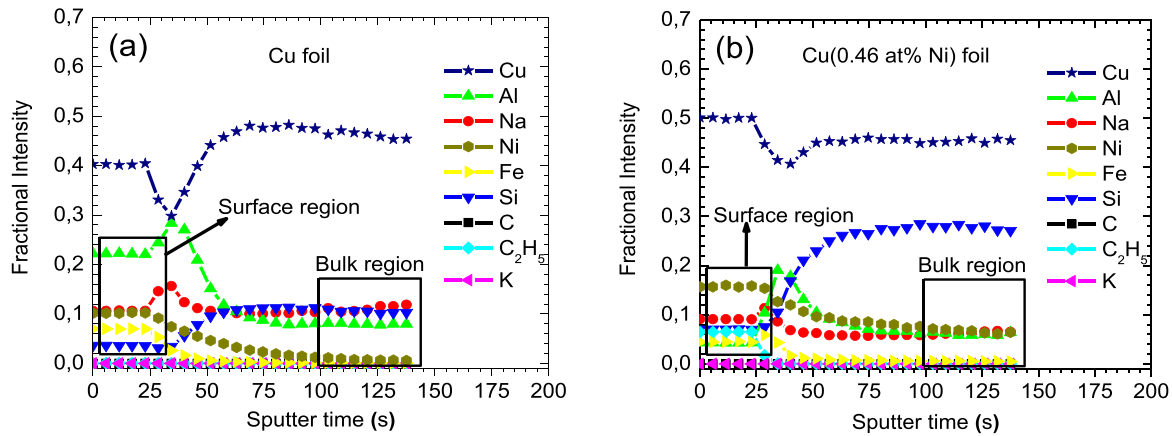
FIG. 5. TOF-SIMS depth profiles of annealed (a) Cu and (b) Cu(0.46 at. % Ni) foils.

due to Ni doped concentration. Also, Si has higher intensity ratio in the bulk of a Cu(0.46 at. % Ni) foil, which does not necessarily mean that Si has higher bulk concentration than Ni, but rather that Si has strong signals in TOF-SIMS. Nevertheless, compared to Cu foil, a higher Si intensity ratio could suggest that during Ni doping process of a Cu an extremely small amount of Si probably from the instrument was introduced as an impurity into the foil, or a measured Si signal was enhanced by ion sputtering during analysis. In both foils, all impurities are expected to have bulk concentrations in the order of few parts per million (≤ 10 ppm) and in Ni doped foil, Ni has $\sim$5000 ppm ($\sim$0.5 at. %). Nevertheless, the TOF-SIMS secondary-ion yield depends strongly on the matrix effects (target chemical and electronic character).

C. Raman characterization of graphene films

Figure 6(a) shows the average spectra of Raman spectra acquired from a $30 \, \mu m^2$ area of graphene films obtained on Cu and Cu(0.46 at. % Ni) foils and transferred onto 300 nm thick SiO_2/Si substrates. The similarity in these average Raman spectra suggests that graphene films obtained on Cu and Cu(0.46 at. % Ni) foils are similar particularly in the number of graphene layers present in the sample. The main features that are observable are labelled, namely, the G-band

mode at $\sim$1590 cm^{-1}, the 2D-band mode at $\sim$2690 cm^{-1}, and the D-band mode at $\sim$1350 cm^{-1} (also known as a disorder-induced band).[1,21] A schematic view in Fig. 6(b) shows that the G-band originates from a normal first-order Raman scattering process in graphene, the 2D-band from a second-order process (double resonance Raman process) that involves two in-plane transverse optical mode (iTO) phonons near the K point, and the D-band from a second-order process that involves one iTO phonon and one defect.[1,21] The Raman process can also give rise to the triple-resonance Raman process, which might explain a more intense 2D-band (relative to the G-band) in monolayer graphene films.[1] By observing the differences in the 2D-band frequency and line shape, the number of graphene layers contained in graphene samples can be obtained and also the stacking order or interlayer interactions in few layers graphene sample.[21,22]

Figures 7(a) and 7(b) Raman data show the 2D peaks Full width at half maximum (FWHM) mapping and the 2D to G peaks intensity ratio (I_{2D}/I_G) mapping, respectively, for graphene films obtained on Cu and Cu(0.46 at. % Ni) foils. *Cu foil graphene*: Fig. 7(a) shows 2D peaks FWHM map with the distribution of the FWHMs in the range of 34–70 cm^{-1}, and in Fig. 7(b) the I_{2D}/I_G peaks intensities ratio is in the range of 0.9–3.0, though Fig. 7(b) shows a range of 0.8–4.4. The symmetric 2D peaks with FWHM in the range
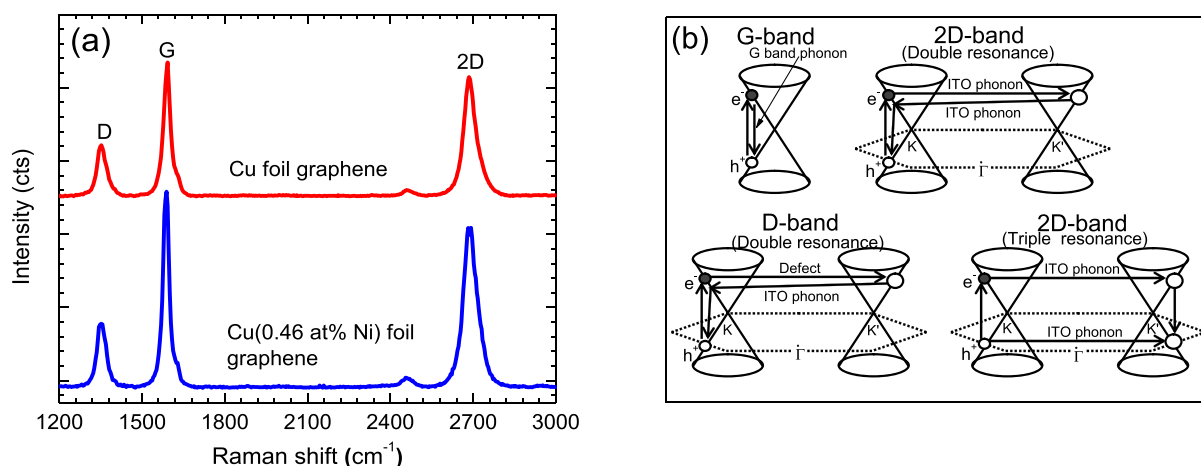

FIG. 6. (a) The average Raman spectra of spectra acquired from a $30 \, \mu m^2$ area of graphene films obtained on Cu and Cu(0.46 at. % Ni) foils and transferred onto SiO_2/Si substrates. (b) A schematic view of Raman scattering processes in graphene film.[1]
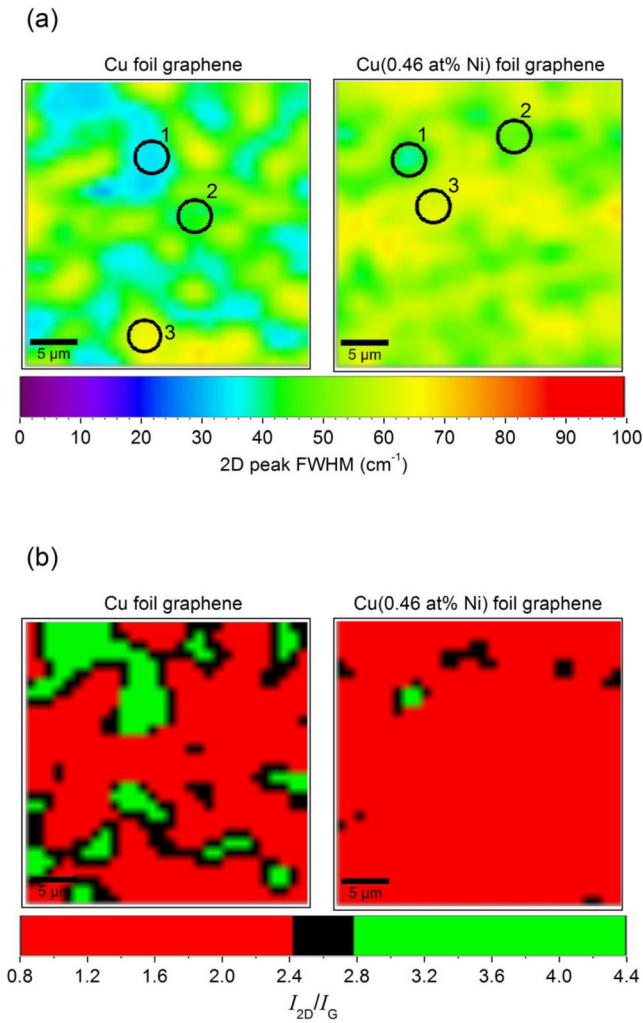
(a)

(b)

FIG. 7. Raman data: (a) The 2D peaks FWHM maps and (b) the 2D to G peaks intensity ratio (I_{2D}/I_G) for graphene films obtained on Cu and Cu(0.46 at. % Ni) foils.

of 28–37 cm^{-1} and the I_{2D}/I_G ratio > 2.5 features demonstrate characteristics of monolayer graphene, and the 2D peaks with FWHM in the range of 38–70 cm^{-1} and the I_{2D}/I_G ratio in the range of 0.5 to <2.5 features demonstrate characteristics of bilayer graphene.[5] Therefore, the bilayer graphene film obtained on Cu foil consists of significant areas of mono and bilayer graphene. *Cu(0.46 at. % Ni) foil graphene*: Fig. 7(a) shows 2D peaks FWHM map with the distribution of the FWHMs is in the range of 37–65 cm^{-1} and the I_{2D}/I_G ratio (Fig. 7(b)) in the range of 0.9–2.8. These features demonstrate characteristics of bilayer graphene, and the 2D peaks with FWHM of 37 cm^{-1} and the I_{2D}/I_G ratio of 2.8 features demonstrate traces of monolayer graphene present in the sample.

As observed in this study, the 2D peaks with the distribution of the FWHMs in the range of approximately 25–70 cm^{-1} and the I_{2D}/I_G peaks intensities ratio in the range of approximately 0.8–4.4 correspond to monolayer and bilayer graphene features. In accordance, a tri or multilayer graphene has 2D peaks with higher FWHMs (>70 cm^{-1}) and lesser I_{2D}/I_G peaks intensities ratio (<0.8).[1,5]

Figure 8 Raman data show the D to G peaks intensity ratio (I_D/I_G) for graphene films obtained on Cu and Cu(0.46
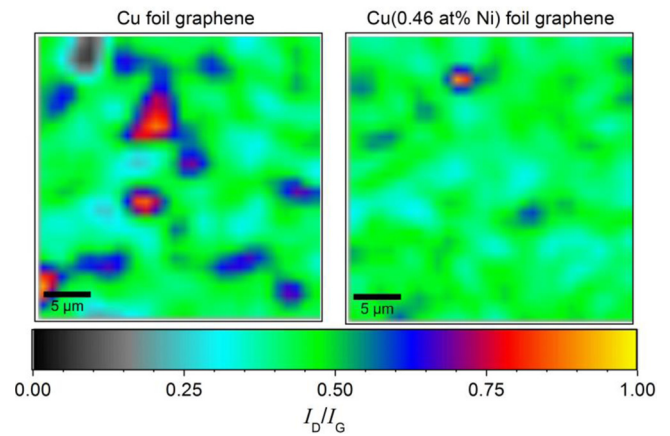

FIG. 8. Raman data: The D to G peaks intensity ratio (I_D/I_G) for graphene films obtained on Cu and Cu(0.46 at. % Ni) foils.

at. % Ni) foils. The graphene films show an I_D/I_G ratio of about 0.5 and suggest that the prepared graphene films are partially defective (have higher D peak intensity relative to the G peak). High D peak intensity shows the presence of impurities or defects in the translational symmetry of the carbon material's lattice, which could be observed under electron diffraction measurements.

Furthermore, the 2D-band mode for monolayer graphene is known to show a single Lorentzian feature.[1] In AB-stacked bilayer graphene, the electronic band is known to split into two components, namely, two conduction and two valence bands where the upper (lower) and lower (upper) branches of the valence (conduction) band are labelled as $\pi_1(\pi_1^*)$ and $\pi_2(\pi_2^*)$, respectively (see a schematic view in Fig. 9(a)).[1,22] The electronic band split results into the splitting of the phonon bands into two components.[22] However, there is only one main double resonance Raman process contributing to the 2D-band. In this double resonance process with respect to the bands split, the electron–phonon scattering occurs with two phonons with symmetries T_1 and T_2. For a T_1 phonon, the scattering can occur between the π_1 and π_1^* or π_2 and π_2^* bands of the same symmetry.[1] For a T_2 phonon, the scattering occurs between bands of different symmetries (i.e., π_1 and π_2^*). T_1 and T_2 phonon processes are labelled as P_{ij}, where i (j) denote an electron scattered from (to) each conduction band $\pi_{i(j)}^*$ (demonstrated in Fig. 9(a)). The P_{11}, P_{22}, P_{12}, and P_{21} scattering processes come from an iTO phonon and give rise to four peaks in the Raman 2D peak spectrum with peak frequencies at approximately 2655, 2680, 2700, and 2725 cm^{-1}, respectively, and FWHMs equal that of monolayer graphene 2D peak.[1] These four peaks are normally fitted as four Lorentzians to 2D peak to demonstrate AB-stacked bilayer graphene.[5,10,22]

The Raman spectra from three spots marked with circles 1, 2, and 3 in Fig. 7(a) are shown in Figs. 9(b) and 9(c). *Cu foil graphene*: In Fig. 9(b), spectrum 1 (from circle 1) has a 2D peak that is single Lorentzian and that shows monolayer graphene. Spectrum 2 (from circle 2) has a 2D peak with larger FWHM of 43 cm^{-1} and is fitted with four Lorentzians each with FWHM of 31 cm^{-1} corresponding to that of a monolayer graphene.[5] The fits demonstrate characteristics of
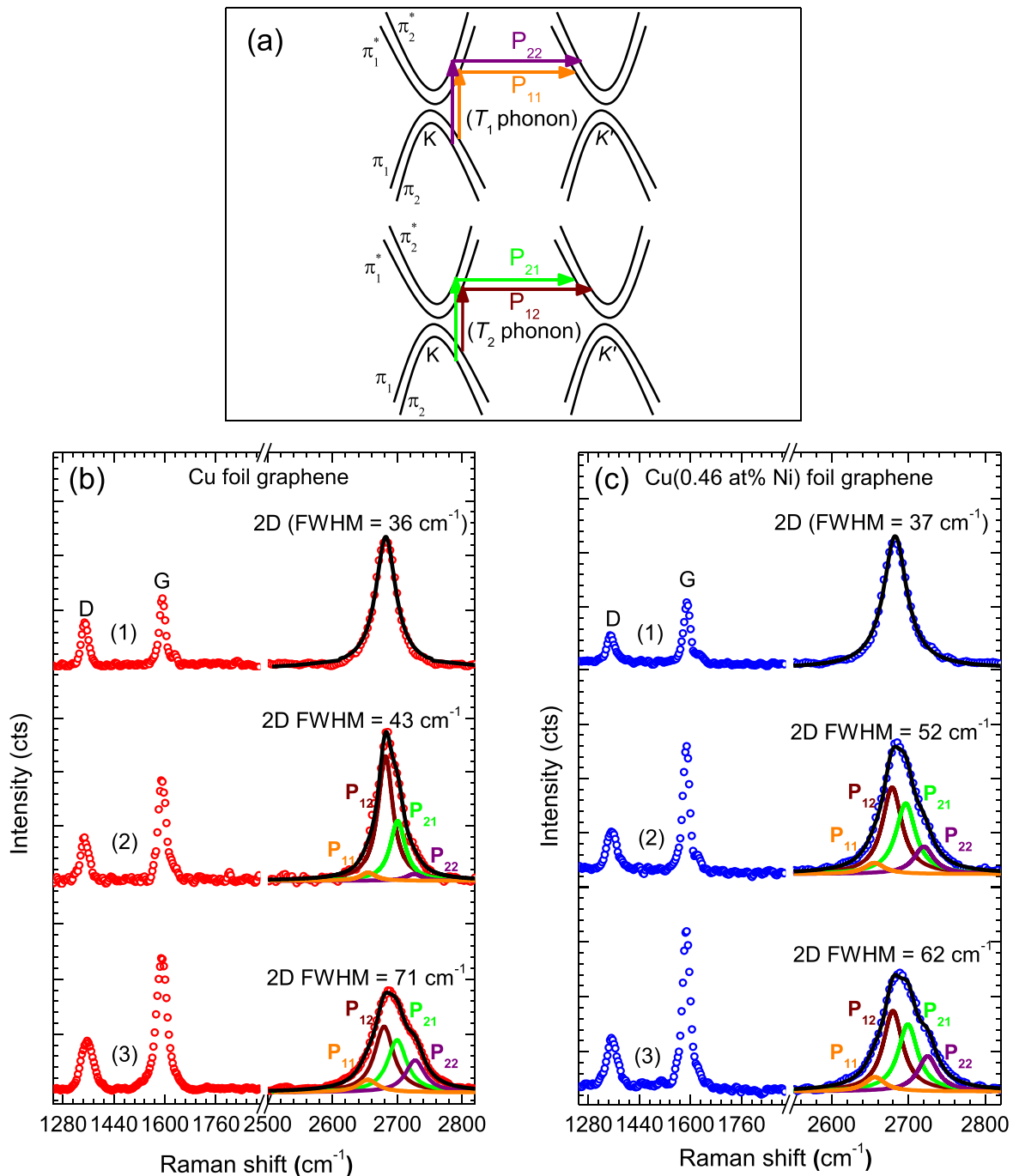
FIG. 9. (a) Schematic view of the electron dispersion of bilayer graphene near the K and K' points showing both π_1 and π_2 bands. The resonance Raman processes are indicated as P_{11}, P_{22}, P_{12}, and P_{21}.[1] (b) and (c) The Raman spectra from three different spots of graphene films obtained on Cu and Cu(0.46 at. % Ni) foils as indicated in Fig. 7(a), respectively.

bilayer graphene that is possibly non-AB stacked due to large differences in relative amplitudes of the Lorentzians. In exfoliated AB-stacked bilayer graphene, the amplitudes of the four Lorentzians are relative, two of which have higher relative intensities (almost the same intensity) than the other two.[22] Nevertheless, the relative amplitudes of the Lorentzians are known to depend on the laser energy,[1] which was maintained constant in this work. Similarly, in spectrum 3 (from circle 3), the 2D peak has larger FWHM of $71 \, \text{cm}^{-1}$ and is fitted with four Lorentzians each with FWHM of $31 \, \text{cm}^{-1}$. The fits demonstrate characteristics of AB-stacked bilayer graphene, since the amplitudes of the four Lorentzians are relative, two of

which have higher relative intensities (almost the same intensity) than the other two.[1,10,22] *Cu(0.46 at. % Ni) foil graphene*: In Fig. 9(c), spectrum 1 (from circle 1) shows single Lorentzian and that shows monolayer graphene. In Spectrum 2 (from circle 2) and 3 (from circle 3), 2D peaks show four Lorentzians each with FWHM of $31 \, \text{cm}^{-1}$. The fits demonstrate characteristics of AB-stacked bilayer graphene. Similar to exfoliated AB-stacked bilayer graphene, the amplitudes of the four Lorentzians are relative.[22] Therefore, a graphene film obtained on Cu(0.46 at. % Ni) foil demonstrates features of a large-area AB-stacked bilayer graphene as compared to graphene film obtained on Cu foil.

Figures 10(a) and 10(b) show the Raman optical micro-scope images of graphene films obtained at a growth temperature of 920 °C on Cu and Cu(0.46 at. % Ni) foils, respectively, and Figs. 10(c) and 10(d) show the images of graphene films obtained at growth temperature of 1000 °C on Cu and Cu(0.46 at. % Ni) foils, respectively (the Raman spectra 1 and 2 (inset to the figures) correspond to areas 1 and 2 (boxes) in images). In Figs. 10(a)–10(c), the Raman spectra from lighter areas (box 1) correspond to that of a monolayer graphene and from darker areas (box 2) to that of bilayer graphene, and also the Raman spectrum in Fig. 10(d) corresponds to that of a bilayer graphene.[22] At a growth temperature of 920 °C, a bilayer graphene obtained on Cu foil shows larger-areas of incomplete bilayer graphene (i.e., monolayer graphene) as compared to bilayer graphene obtained on Cu(0.46 at. % Ni) foil. At a growth temperature of 1000 °C, a bilayer graphene obtained on Cu foil is also incomplete (has small-areas of bilayer on a monolayer graphene background), and bilayer graphene obtained on Cu(0.46 at. % Ni) foil shows a large-area (or wafer-scale) bilayer graphene with a much better or high-quality graphene. Clearly, the optical microscope images suggest that the bilayer graphene growth rate on Cu(0.46 at. % Ni) foil is higher as compared to Cu foil.

D. Four point probe graphene film sheet resistance

In a four-point probe/sheet resistance measuring system for thin films, two electrodes are used for sourcing a DC current, I (through the outer two probes) and the other two for measuring the corresponding voltage drop, V (see a schematic view, i.e., inset to Fig. 11(a)). Figure 11(a) shows the measured voltage drop for bilayer graphene films obtained on Cu and Cu(0.46 at. % Ni) foils and that was used to calculate the sheet resistance of graphene films (Fig. 11(b)) using an approach which relies on a geometric factor. A bilayer graphene film obtained on a Cu foil shows a high sheet resistance (380 Ω/sq) as compared to that obtained on Cu(0.46 at. % Ni) foil (315 Ω/sq) and that could be as a result of larger areas of incomplete bilayer graphene (i.e., monolayer graphene areas) present in a film obtained on Cu foil as compared to that obtained on Cu(0.46 at. % Ni) foil, since sheet resistance decreases with the increase in graphene film thickness or number of graphene layers.

E. Electron diffraction of graphene film obtained on Cu(Ni) foil

Figure 12(a) shows the TEM image of the graphene film obtained on Cu(0.46 at. % Ni) foil and transferred onto the
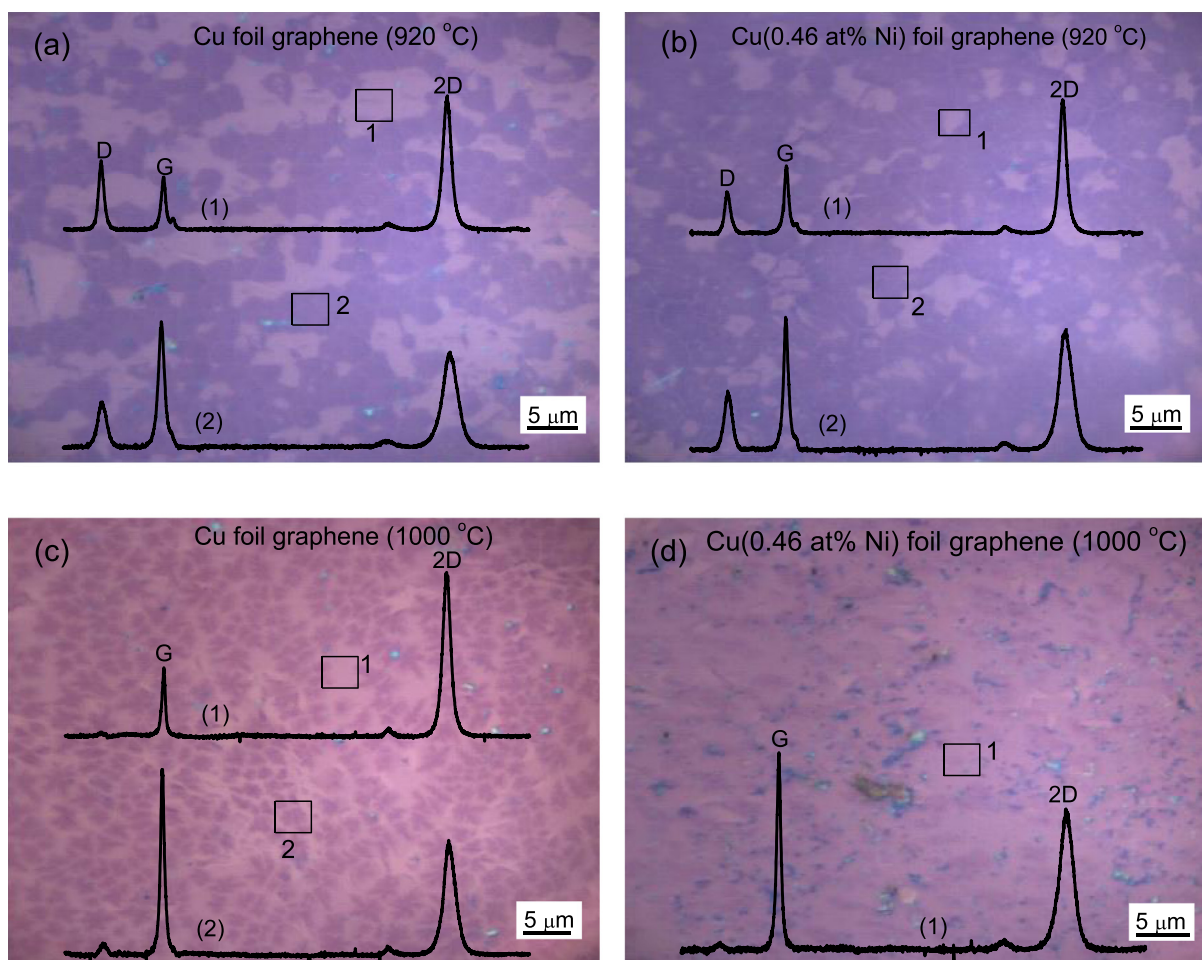

FIG. 10. The Raman optical microscope images (100×/0.90 objective) of graphene films obtained on (a) Cu and (b) Cu(0.46 at. % Ni) foils at 920 °C and on (c) Cu and (d) Cu(0.46 at. % Ni) foils at 1000 °C (transferred onto 300 nm thick SiO$_2$/Si substrate. The inset: Raman spectra corresponding to areas indicated as boxes 1 and 2.
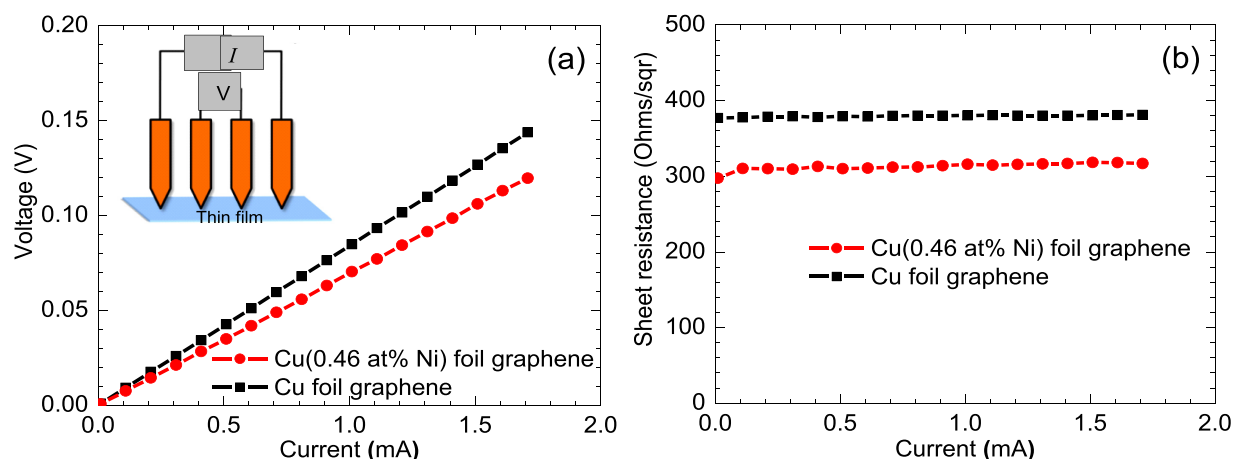
FIG. 11. (a) A four point probe measured voltage drop for bilayer graphene films obtained on Cu and Cu(0.46 at. % Ni) foils and (b) the calculated sheet resistance of the corresponding graphene films.

TEM Cu grid. Figure 12(b) inset shows the electron diffraction pattern that shows two sets of diffraction rings. The diffraction patterns were analysed with diffraction ring profiler (which was developed for phase identification in complex microstructures[23] to obtain the diffraction intensity profile (Fig. 12(b)) which shows two peaks at an inter-planar spacing of $d = 1.23$ Å (outer ring) and $d = 2.13$ Å (inner ring) corresponding to indices (1–210) and (1–110), respectively.[24] The relative intensity of the spots in the outer ring is twice that of the spots in the inner ring and that demonstrates AB stacking order.[10,22,24] The selected area electron diffraction method confirms the bilayer graphene with AB stacking and that corresponds to the bilayer graphene features observed from Raman data (i.e., 2D peaks FWHMs and peaks intensities ratio).

IV. DISCUSSION

In prepared dilute Cu(Ni) foils, Ni is uniformly distributed and the Ni content present in Cu foil (un-doped) is due to Cu foil impurities, since Alfa Aesar Cu foil for graphene growth with purity of 99.8% has about 0.2% unknown-impurities. Interestingly, Ni in Cu foils showed surface

precipitation/segregation capability which is expected to enhance bilayer graphene coverage rate by enhancing the methane decomposition rate of Cu in CVD graphene growth. In CVD graphene growth on Cu foil, only the surface of a foil is important, since a growth is limited to surface reaction.[4] Meaning, in the early stage of graphene growth, the interaction between the hydrocarbon and the Cu substrate is important. Despite that the Cu-graphene interaction is relatively weak after growth, hence graphene is easily transferable from Cu substrate.[4,6] It is known that the surface orientation of the Cu foil influences the graphene growth rate and the number of layers in graphene film.[6] Studies have shown that the Cu(100) surface causes multilayer graphene growth, and high index Cu surface orientations cause compact graphene island formation with growth rates higher than those on Cu(100).[6,25] In this work, an Alfa Aesar Cu foil for graphene growth with (001) surface orientation/lattice plane which is equivalent to Cu(100) plane will have a preferential growth of multilayer graphene.[6,25] On ideal flat Cu surface, a single (001) surface orientation of a Cu foil will lead to a uniform growth rate in early stages of graphene growth. However, a high degree of uniform distribution of islands (uniform growth rate) on Cu surface is affected by an amount
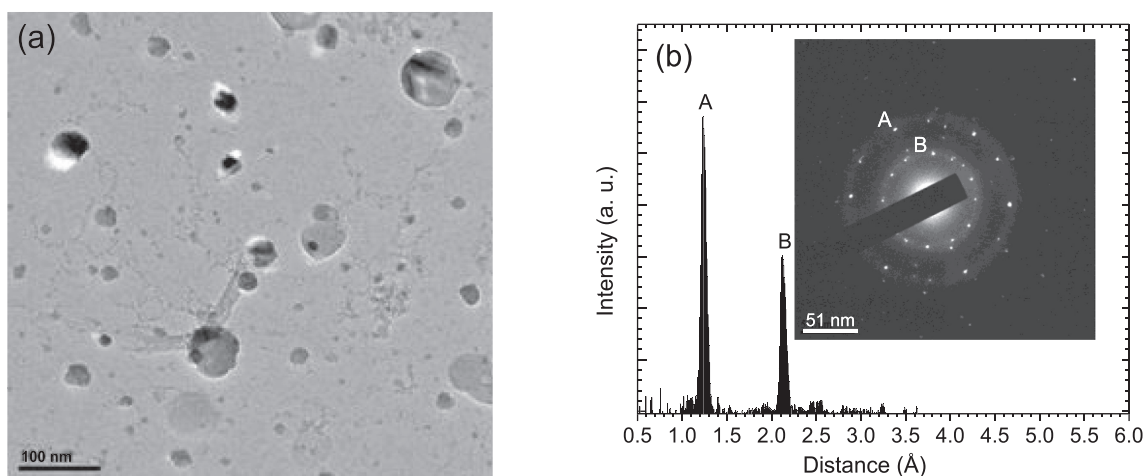

FIG. 12. (a) TEM image of the graphene film obtained on Cu(0.46 at. % Ni) foil at growth temperature of 920 °C and transferred onto TEM Cu grid. (b) The electron diffraction intensity profile of the diffraction pattern (inset to the figure) of the graphene film obtained on Cu(0.46 at. % Ni) foil.

of imperfection sites (the sharp structures) on Cu surface that are not completely removed during high-temperature annealing under hydrogen and argon gas flow. In addition, a single Cu surface orientation also leads to a uniform Ni surface concentration distribution through segregation kinetics.[26] In prepared dilute Cu(Ni) foil, the maximum surface concentration of Ni that segregated during CVD graphene growth is determined by Ni concentration in Cu (i.e., Ni bulk concentration) and Ni segregation driving energy (segregation energy). More precisely, the surface enrichment of Ni in dilute Cu(Ni) foil is driven by a change in chemical potential energy (writeable in terms of the segregation energy, ΔG), which results in the minimization of the total energy of the crystal.[26] Part of the modified Darken equations, which defines the rate of surface concentration build-up of dope element 1 (e.g., Ni in dilute Cu(Ni) foil), is[26]

$$\frac{\partial X_1^{\phi}}{\partial t} = \frac{M_1 X_1^{B_1}}{d^2} \left[\Delta G + RT \ln \frac{X_1^{B_1}\left(1 - \frac{X_1^{\phi}}{X^M}\right)}{\frac{X_1^{\phi}}{X^M}\left(1 - X_1^{B_1}\right)} \right], \quad (2)$$

where X_1^{ϕ} is the surface concentration of the segregating dope element 1, X_1^B is the bulk concentration, X^M is the maximum surface concentration <100 at. %, M_1 is the mobility, d is the thickness of the segregated layer, R is the gas constant, and T is the temperature.

In Eq. (2), as the crystal temperature increases, surface concentration build-up of dope element 1 increases until it reaches a maximum surface concentration (i.e., segregation equilibrium), then, a further increase in temperature results in desegregation. At equilibrium, $\partial X_1^{\phi}/\partial t = 0$ and Eq. (1) reduces to the Langmuir–McLean equation[26]

$$\frac{X_1^{\phi}/X^M}{1 - X_1^{\phi}/X^M} = \frac{X_1^B}{1 - X_1^B} \exp\left(\frac{-\Delta G}{RT}\right). \quad (3)$$

From a well-known thermodynamic expression, $\Delta G = \Delta H - T\Delta S$, where ΔH is segregation enthalpy, T is temperature, and ΔS is segregation entropy.[27] In a dilute system, the segregation entropy (ΔS) is negligible (generally $\Delta S/R < 1$) and $\Delta G \approx \Delta H$.[28] The segregation enthalpy can be approximated by[26,27]

$$\Delta H = \left(\frac{\Delta Z}{Z}\right)\left(\Delta H_B^{sub} - \Delta H_A^{sub}\right), \quad (4)$$

where Z is bulk coordination number ($Z = 12$ for Cu crystal), ΔZ is a difference in coordination number between bulk and surface ($\Delta Z = 4$ for Cu(001)), ΔH^{sub} is the heat of sublimation for element A and B ($\Delta H_{Cu}^{sub} = 339.3$ kJ/mol and $\Delta H_{Ni}^{sub} = 430.1$ kJ/mol (Refs. 29 and 30)). For a dilute Cu(001)(Ni) alloy, $\Delta H = 30.3$ kJ/mol (from Eq. (4)), and therefore, $\Delta G = 30.3$ kJ/mol. Now, substituting $\Delta G = 30.3$ kJ/mol in Eq. (3), the temperature dependence of the Ni surface concentration in dilute Cu(Ni) alloy was obtained (Fig. 13) for $X_1^B = 0.3$, 0.5, 0.7, and 0.9 at. % Ni and $X^M = 25$ at. %. (Low energy electron diffraction over-structures have shown that the maximum surface
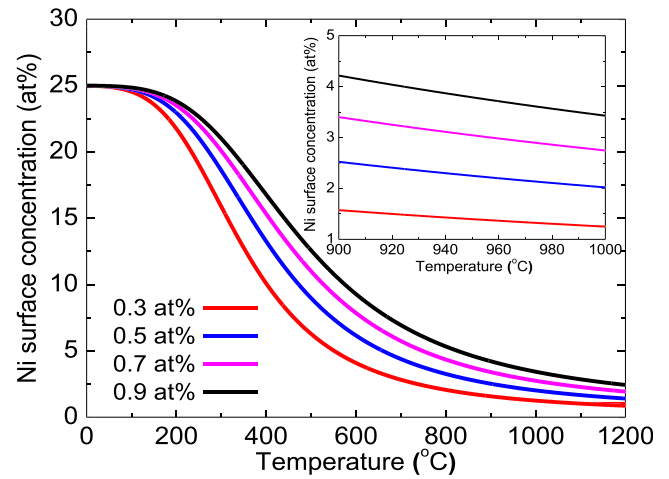

FIG. 13. The temperature dependence of the Ni surface concentration in dilute Cu(Ni) alloy obtained with Langmuir–McLean equation, the inset shows the same plot in temperature range of 900–1000 °C.

concentration of a substitutional segregating dope element for a Cu(001) is 25 at. % (Ref. 31).) The CVD graphene growths on Cu are carried-out in the temperature range of 900–1000 °C, and in this temperature range (see the inset to Fig. 13), the maximum surface concentration of Ni in dilute Cu(Ni) alloy is in the range of 1 to <5 at. %. At a growth temperature of 920 °C, a surface layer of a dilute Cu(0.46 at. % Ni) foil is expected to have a composition of about 2 at. % Ni and 98 at. % Cu. In the study of Liu *et al.*,[5] a Cu(1200 nm)/Ni(400 nm) thin film with a surface layer composition of about more than 97 at. % Cu and lesser than 3 at. % Ni at a CVD growth temperature of 920 °C demonstrated a capability of producing large-area AB-stacked bilayer graphene film. Accordingly, a dilute Cu(0.46 at. % Ni) foil has demonstrated a capability of producing large-area AB-stacked bilayer graphene film as compared to Cu foil (see the above discussion on Raman data).

It could be expected that a proposed surface layer composition of a dilute Cu(0.46 at. % Ni) foil will be altered by Cu sublimation during CVD graphene growth. For instance, in low-pressure CVD, annealing at high temperatures ≥ 1000 °C leads to a significant increase in the rate of Cu sublimation.[32] However, in atmospheric pressure CVD at the same annealing temperatures (i.e., ≥ 1000 °C), the rate of Cu sublimation is expected to decrease significantly. In fact, at higher pressures, the sublimation of Cu is suppressed.[33]

Furthermore, under optimised AP-CVD graphene growth conditions, a bilayer graphene obtained on Cu foil showed larger-areas of incomplete bilayer graphene (i.e., small-areas of bilayer on a monolayer graphene background) as compared to large-area (or wafer-scale) bilayer graphene obtained on Cu(0.46 at. % Ni) foil and that could be due to graphene growth rate which is expected to be higher on Cu(0.46 at. % Ni) foil as compared to Cu foil, following from the enhancement of methane decomposition rate of Cu by Ni. Generally, a slower crystal growth rate yields few crystalline dislocations, and the non-AB stacking in bilayer graphene is due to the undesired dislocations between two graphene layers.[34] Therefore, a slower graphene growth rate

observable on Cu as compared to Cu(Ni) could contribute significantly to crystalline dislocations (non-AB stacking) in bilayer graphene. Nonetheless, a bilayer graphene film obtained on Cu compared to Cu-Ni alloy is known to have a significant fraction of non-AB stacking.[4,5,10] The incomplete bilayer graphene coverage though could also be viewed as an effect of H$_2$ etching during annealing;[32] in this study, an attempt to suppress or minimise the annealing effects of H$_2$ on as-grown graphene includes a rapid cooling of as-grown graphene/Cu samples. Nonetheless, H$_2$ effects in CVD graphene growth have positive effects. For instance, the effect of H$_2$ in CVD graphene growth was viewed as a co-catalyst in the formation of active surface bound carbon species required for graphene growth[32,35,36] and etches away the weak carbon-carbon bonds (graphene edges) for the growth of bilayer or multilayer graphene.[33,37] The effects of H$_2$ are expected to be the same for graphene films obtained on both Cu and Cu(0.46 at. % Ni) foils, since the two are synthesized simultaneously. Though CVD graphene growth on Cu surface is a catalytic process which has simplicity view, the CVD growth mechanism is complicated and depends on growth background pressure. Generally, on the Cu surface where the decomposition of hydrocarbons and the surface diffusion induced graphene growth materialise, several processes are involved which includes:[4,33,38,39]

(i)   Absorption and desorption of hydrocarbon molecules on Cu.
(ii)   Decomposition of hydrocarbon to form active carbon species.
(iii)   Aggregation of carbon species on Cu surface (i.e., formation of nucleation sites).
(iv)   Surface diffusion and attachment of carbon species to nucleation sites to materialise graphene.
(v)   Etching of the as-grown graphene, etc.

Due to simultaneous CVD growth of graphene on both Cu and Cu(0.46 at. % Ni) foils, all the above-mentioned processes are expected to be the same for both Cu and Cu(0.46 at. % Ni) foils, but except for the second process (i.e., decomposition of hydrocarbon to form active carbon species). A process of the decomposition of hydrocarbon to form active carbon species could be viewed as a supply of active carbon species for graphene to materialise. Once more, as compared to Cu, Ni has higher methane decomposition rate (i.e., supply of active carbon species) and higher carbon solubility.[5,40,41] Hence, contrary to Cu, Cu(0.46 at. % Ni) foil can be expected to easily decompose hydrocarbons and provide sufficient carbon species for bilayer or multilayer graphene growth. In this instance, the assumption is that graphene growth on both Cu and dilute Cu(0.46 at. % Ni) foils occurs mostly during the hydrocarbon exposure at a constant temperature, rather than due to carbon precipitation/segregation during cooling.[5,42] Despite the assumption, carbon has very low solubility in Cu (<0.001 at. % at 1000 °C),[43] and for carbon to precipitate during cooling an equilibrium saturation of carbon atoms in Cu substrate is required,[26] which may not be possible since the CVD growth of graphene (i.e., Cu substrate exposure to carbon source) occurs over few minutes.[44,45] In addition, Harpale *et al.*[45]

has demonstrated that carbon diffusion into Cu is restricted by preferential carbon-carbon bonds formation (carbon-carbon dimer pairs) over Cu-carbon bonds. Hence, graphene growth on Cu can be regarded to occur mostly during the hydrocarbon exposure at a constant temperature. At graphene growth temperatures (∼1000 °C), a surface layer of a dilute Cu(0.46 at. % Ni) foil is expected to have a higher relative surface concentration of Ni due to Ni segregation.[26] In contrary to a surface layer of a dilute Cu(0.46 at. % Ni) foil, a subsurface layer is expected to have ∼0 at. % Ni, since Ni enrichment of a surface layer of a dilute Cu(0.46 at. % Ni) foil will deplete the subsurface layer(s).[26] As a result, during exposure to carbon source, a surface layer of a dilute Cu(0.46 at. % Ni) foil will have both Cu-carbon and Ni-carbon bonds/interaction effects, and a subsurface layer which is mostly Cu will have preferential carbon-carbon bonds (which restrict carbon diffusion into Cu)[45] and very low carbon solubility similar to Cu. Similarly, graphene growth on dilute Cu(0.46 at. % Ni) foil can be regarded to occur mostly during the hydrocarbon exposure at a constant temperature. During CVD graphene growth, unlike Cu surface, the metal-carbon interaction effects of a dilute Cu(0.46 at. % Ni) foil surface will have both Cu-carbon and Ni-carbon interactions effects, hence a dilute Cu(0.46 at. % Ni) foil is expected to easily decompose hydrocarbons and supply sufficient active carbon species for bilayer or multi-layer graphene growth.

In previous studies, it is mentioned that a CVD substrate with a surface layer elemental composition of about 97 at. % Cu and 3 at. % Ni grows bilayer graphene with an AB-stacked yield in the range of 95%–100%, which is attributed to the surface catalytic graphene growth mode with a certain methane decomposition rate[5] and AP-CVD graphene growth on Cu substrate grow small-areas of multilayer graphene on a monolayer graphene background at higher methane concentrations (low methane concentrations grow wafer-scale monolayer graphene).[41] The capability of Cu-Ni alloy to grow large-area AB-stacked bilayer graphene as compared to Cu which is known to grow islands of bilayer graphene with a significant fraction of non-AB stacking is discussed on the basis of metal-carbon solubility and hydrocarbon decomposition rate.[4–6]

In addition, a discussion on the driving energy or mechanism behind a favorable growth of AB-stacked graphene layers on Cu-Ni alloy as compared to Cu is lacking in literature, and also this study does not have supported results to give such detailed discussion. Nonetheless, if a thermodynamic process driving a Bernal stacking of two superimposed graphene layers is viewed as a minimization of the total energy of a metal-carbon (graphene) system. Therefore, as compared to preferential carbon-carbon interactions over Cu-carbon interactions in Cu, preferential Ni-carbon interactions over Cu-carbon and carbon-carbon interactions in Cu-Ni alloy[45] suggest that a Cu-Ni-carbon system has lowest crystal energy over a Cu-carbon system, which makes it a favourable system for thermodynamic process driving a Bernal stacking of two superimposed graphene layers.

The sheet resistance obtained for bilayer graphene film obtained on a Cu(0.46 at. % Ni) foil (315 Ω/sq) compares

well with that of a large area bilayer graphene (287 Ω/sq) obtained by Chen *et al.*[6] using non-dilute commercial Cu-Ni alloy foils. The Raman and electron diffraction data showed that the graphene film obtained on Cu(0.46 at. % Ni) foil is mainly AB-stacked bilayer graphene.

Once more, Alfa Aesar Cu foils for graphene growth with purity of 99.8% have about 0.2% unknown-impurities, and Liu *et al.*[4] have demonstrated that the purity of Cu surface plays a critical role in determining the number of graphene layers. In this study, un-doped and Ni doped Cu foils are obtained from the same Alfa Aesar Cu foil, hence they have the same amount and type of unknown-impurities. So, the effect of these unknown-impurities in graphene growth is the same for both foils under the same growth conditions; hence, the effect can be ruled-out in comparison of graphene films obtained from both un-doped and Ni doped Cu foils. Though this study focuses on CVD bilayer graphene growth, the advantage of CVD technique for controlling graphene layer thickness can further be expanded to uniform multi-layer graphene growth in comparison to multi-layer graphene synthesized using chemical methods for anode material in Li-ion batteries.[46,47]

V. CONCLUSIONS

This study demonstrated the solid state diffusion doping of annealed Cu foils for graphene growth with small concentrations of Ni to obtain a dilute Cu(Ni) alloy in which the hydrocarbon decomposition rate of Cu will be enhanced by Ni during synthesis of large-area AB-stacked bilayer graphene using AP-CVD setup. As compared to Cu foil, the prepared dilute Cu(Ni) alloy demonstrated the good capability of growing large-area AB-stacked bilayer graphene by increasing Ni content in Cu surface layer thus altering a composition of a Cu surface where the decomposition of hydrocarbons and the surface diffusion induced graphene growth materialise. The methane decomposition rate of Cu surface for large-area CVD bilayer graphene growth was engineered with Ni through a well-known segregation phenomenon. The number of graphene layers contained in films and the AB stacking order of synthesized graphene films were confirmed by Raman and electron diffraction pattern measurements. The results obtained in this work demonstrated the interest and potential insight of using dilute Cu(Ni) alloy as a substrate in AP-CVD for synthesis of a large-area AB-stacked bilayer graphene film.

ACKNOWLEDGMENTS

[1]*Physics of Graphene*, edited by H. Aoki and M. S. Dresselhaus (Springer, New York, 2014).
[2]Y. Zhang, T. Tang, C. Girit, Z. Hao, M. C. Martin, A. Zettl, M. F. Crommie, Y. R. Shen, and F. Wang, Nature **459**, 820 (2009).
[3]W. J. Yu, L. Liao, S. H. Chae, Y. H. Lee, and X. Duan, Nano Lett. **11**, 4759 (2011).
[4]W. Liu, H. Li, C. Xu, Y. Khatami, and K. Banerjee, Carbon **49**, 4122 (2011).
[5]W. Liu, S. Kraemer, D. Sarkar, H. Li, P. M. Ajayan, and K. Banerjee, Chem. Mater. **26**, 907 (2014).
[6]S. Chen, W. Cai, R. D. Piner, J. W. Suk, Y. Wu, Y. Ren, J. Kang, and R. S. Ruoff, Nano Lett. **11**, 3519 (2011).
[7]H. Choi, Y. Lim, M. Park, S. Lee, Y. Kang, M. S. Kim, J. Kim, and M. Jeon, J. Mater. Chem. C **3**, 1463 (2015).
[8]C. Mattevi, H. Kim, and M. Chhowalla, J. Mater. Chem. **21**, 3324 (2011).
[9]N. Liu, L. Fu, B. Dai, K. Yan, X. Liu, R. Zhao, Y. Zhang, and Z. Liu, Nano Lett. **11**, 297 (2011).
[10]W. Fang, A. L. Hsu, R. Caudillo, Y. Song, A. G. Birdwell, E. Zakar, M. Kalbac, M. Dubey, T. Palacios, M. S. Dresselhaus, P. T. Araujo, and J. Kong, Nano Lett. **13**, 1541 (2013).
[11]U. Vahalia, P. A. Dowben, and A. Miller, J. Vac. Sci. Technol., A **4**(3), 1675 (1986).
[12]A. Reina, X. Jia, J. Ho, D. Nezich, H. Son, V. Bulovic, M. S. Dresselhaus, and J. Kong, Nano Lett. **9**(1), 30 (2009).
[13]X. Liu, L. Fu, N. Liu, T. Gao, Y. Zhang, L. Liao, and Z. Liu, J. Phys. Chem. C **115**, 11976 (2011).
[14]Y. Wu, H. Chou, H. Ji, Q. Wu, S. Chen, W. Jiang, Y. Hao, J. Kang, Y. Ren, R. D. Piner, and R. S. Ruoff, ACS Nano **6**(9), 7731 (2012).
[15]S. Lee, K. Lee, and Z. Zhong, Nano Lett. **10**, 4702 (2010).
[16]S. M. Kim, A. Hsu, Y. H. Lee, M. Dresselhaus, T. Palacios, K. K. Kim, and J. Kong, Nanotechnology **24**, 365602 (2013).
[17]J. Crank, *The Mathematics of Diffusion*, 2nd ed. (Clarendon Press, Oxford, 1975).
[18]W. Gale and T. Totemeier, *Smithells Metals Reference Book*, 8th ed. (Elsevier Butterworth-Heinemann, Ltd., Oxford, UK, 2004).
[19]M. Fabiane, "Chemical vapour deposition of graphene: Fundamental aspects of synthesis and characterization," Ph.D. thesis (University of Pretoria, South Africa, 2014).
[20]M. Her, R. Beamsa, and L. Novotnya, Phys. Lett. A **377**, 1455 (2013).
[21]L. M. Malard, M. A. Pimenta, G. Dresselhaus, and M. S. Dresselhaus, Phys. Rep. **473**, 51 (2009).
[22]A. C. Ferrari, J. C. Meyer, V. Scardaci, C. Casiraghi, M. Lazzeri, F. Mauri, S. Piscanec, D. Jiang, K. S. Novoselov, S. Roth, and A. K. Geim, Phys. Rev. Lett. **97**, 187401 (2006).
[23]L. Zhang, C. M. B. Holt, E. J. Luber, B. C. Olsen, H. Wang, M. Danaie, X. Cui, X. Tan, V. Lui, W. P. Kalisvaart, and D. Mitlin, J. Phys. Chem. C **115**, 24381 (2011).
[24]A. Dato, V. Radmilovic, Z. Lee, J. Phillips, and M. Frenklach, Nano Lett. **8**(7), 2012 (2008).
[25]J. D. Wood, S. W. Schmucker, A. S. Lyons, E. Pop, and J. W. Lyding, Nano Lett. **11**, 4547 (2011).
[26]J. Du Plessis, *Solid State Phenomena—Part B*, Diffusion and Defect Data Vol. 11 (Sci-Tech Publications, Brookfield, USA, 1990).
[27]S. Stølen and T. Grande, *Chemical Thermodynamics of Materials* (John Wiley & Sons, Ltd., 2004).
[28]S. Hofmann and R. Frech, Anal. Chem. **57**, 716 (1985).
[29]*CRC Handbook of Chemistry and Physics*, 63rd ed., edited by R. C. Weast and M. J. Astle (CRC Press, Inc., 1982).
[30]K. Wandelt and C. R. Brundle, Phys. Rev. Lett. **46**, 1529 (1982).
[31]S. Higashi, H. Tochihara, V. L. Shneerson, and D. K. Saldin, Surf. Sci. **602**, 2473 (2008).
[32]P. R. Kidambi, C. Ducati, B. Dlubak, D. Gardiner, R. S. Weatherup, M. Martin, P. Seneor, H. Coles, and S. Hofmann, J. Phys. Chem. C **116**, 22492 (2012).
[33]I. Vlassiouk, S. Smirnov, M. Regmi, S. P. Surwade, N. Srivastava, R. Feenstra, G. Eres, C. Parish, N. Lavrik, P. Datskos, S. Dai, and P. Fulvio, J. Phys. Chem. C **117**, 18919 (2013).
[34]A. W. Robertson, A. Bachmatiuk, Y. A. Wu, F. Schäffel, B. Rellinghaus, B. Büchner, M. H. Rümmeli, and J. H. Warner, ACS Nano **5**(8), 6610 (2011).
[35]D. H. Jung, C. Kang, M. Kim, H. Cheong, H. Lee, and J. S. Lee, J. Phys. Chem. C **118**, 3574 (2014).
[36]M. Losurdo, M. M. Giangregorio, P. Capezzuto, and G. Bruno, Phys. Chem. Chem. Phys. **13**, 20836 (2011).
[37]X. Zhang, L. Wang, J. Xin, B. I. Yakobson, and F. Ding, J. Am. Chem. Soc. **136**, 3040 (2014).

[38]P. Lenzsolomun, M. C. Wu, and W. Goodman, Catal. Lett. **25**, 75 (1994).

[39]J. A. Venables, G. D. T. Spiller, and M. Hanbucken, Rep. Prog. Phys. **47**, 399 (1984).

[40]W. Cai, R. D. Piner, Y. Zhu, X. Li, Z. Tan, H. C. Floresca, C. Yang, L. Lu, M. J. Kim, and R. S. Ruoff, Nano Res. **2**, 851 (2009).

[41]S. Bhaviripudi, X. Jia, M. S. Dresselhaus, and J. Kong, Nano Lett. **10**, 4128 (2010).

[42]R. Muñoz and C. Gómez-Aleixandre, Chem. Vap. Deposition **19**, 297 (2013).

[43]G. A. López and E. J. Mittemeijer, Scr. Mater. **51**, 1 (2004).

[44]J. J. Lander, H. E. Kern, and A. L. Beach, J. Appl. Phys. **23**, 1305 (1952).

[45]A. Harpale, M. Panesi, and H. B. Chew, J. Chem. Phys. **142**, 061101 (2015).

[46]S. Petnikota, N. K. Rotte, M. V. Reddy, V. V. S. S. Srikanth, and B. V. R. Chowdari, ACS Appl. Mater. Interfaces **7**, 2301 (2015).

[47]S. Petnikota, N. K. Rotte, V. V. S. S. Srikanth, B. S. R. Kota, M. V. Reddy, K. P. Loh, and B. V. R. Chowdari, J. Solid State Electrochem. **18**, 941 (2014).